

Carbonate rocks: Matrix permeability estimation

Alejandro Cardona and J. Carlos Santamarina

ABSTRACT

Carbonate rocks store half of the world's proven oil reserves. Genesis and postdepositional diagenetic processes define the porous network topology and the matrix permeability. This study compiles a database of porosity, specific surface, mercury porosimetry, and permeability values extracted from published sources and complements the database through a focused experimental study. Specific surface and porosity combine to estimate the pore size (D_{sur}). Permeability versus D_{sur} data cluster along a single trend with a slope of 2 in a log-log scale, which is in agreement with the Kozeny-Carman model. Discordant data points correspond to samples with dual porosity or broad pore-size distributions with long tails, where flow channels along larger interconnected pores. Indeed, the detailed analysis of all the porosimetry data in the database shows that permeability correlates best with the pore size D80, that is, the 80th percentile in pore-size distributions. Once again, the best fit is a power function in terms of $(D80)^2$, analogous to Kozeny-Carman. The prediction uncertainty using D80 is one order of magnitude and has the same degree of uncertainty as more complex models and analyses. This observation suggests an irreducible uncertainty of one order of magnitude in permeability estimation from index properties such as porosity, mercury porosimetry, and specific surface probably resulting from specimen preparation effects, inherent physical differences in permeation versus invasion, and difficulties in data interpretation. These estimates of permeability are most valuable when specimens are limited to small sizes, such as cuttings.

INTRODUCTION

The world energy demand has steadily increased during the last century, with an additional 30% increase in demand predicted

Copyright ©2020. The American Association of Petroleum Geologists. All rights reserved. Green Open Access. This paper is published under the terms of the CC-BY license.

Manuscript received September 16, 2017; provisional acceptance October 31, 2017; revised manuscript received March 18, 2018; revised manuscript provisional acceptance April 26, 2018; 2nd revised manuscript received July 8, 2018; 2nd revised manuscript provisional acceptance October 29, 2018; 3rd revised manuscript received January 14, 2019; 3rd revised manuscript provisional acceptance January 30, 2019; 4th revised manuscript received February 19, 2019; final acceptance May 2, 2019.
DOI:10.1306/05021917345

AUTHORS

ALEJANDRO CARDONA ~ *Energy Resources and Petroleum Engineering, King Abdullah University of Science and Technology (KAUST), Thuwal, Saudi Arabia;*
alejandro.cardonaramirez@kaust.edu.sa

Alejandro Cardona received his M.Sc. from KAUST and his B.S. from the Universidad Nacional de Colombia. He is currently pursuing his doctoral studies in energy resources and petroleum engineering at KAUST. His research focuses on the understanding of flow-related phenomena in porous media with an emphasis on fractured carbonate rocks.

J. CARLOS SANTAMARINA ~ *Energy Resources and Petroleum Engineering, KAUST, Thuwal, Saudi Arabia;*
carlos.santamarina@kaust.edu.sa

Juan Carlos Santamarina received his Ph.D. from Purdue University, his M.Sc. from the University of Maryland, and his CE from Universidad Nacional de Córdoba Argentina. He explores the foundations of subsurface processes using particle- and pore-scale testing methods combined with high-resolution geophysical process monitoring systems and inversion techniques. The combined experimental-numerical framework supports developments in the field of energy geotechnology, with contributions to resource recovery as well as energy and waste geostorage.

ACKNOWLEDGMENTS

Support for this research was provided by the King Abdullah University of Science and Technology Endowment. G. E. Abelskamp edited the manuscript.

DATASHARE 115

Table S1 is available in an electronic version on the AAPG website (www.aapg.org/datashare) as Datashare 115.

by the year 2040 (BP, 2018). Fossil fuels satisfy 81% of the current global energy consumption (International Energy Agency, 2018). Although its share of the total consumption will decrease to 75% by the midcentury, the actual consumption of nonrenewable sources will continue to increase. Hydrocarbons comprise half of the global energy mix (International Energy Agency, 2015).

The rock porosity and permeability determine the quality of hydrocarbon reservoirs: porosity implies storage capacity, whereas permeability is needed for flow and recovery (Dullien, 1992; Tiab and Donaldson, 2012). Natural and induced fractures control the overall flow in carbonate reservoirs (Van Golf-Racht, 1996; Gale et al., 2004; Ortega et al., 2010); however, the rate at which stored hydrocarbons exit the matrix into fractures depends on the matrix permeability.

Permeability relates the average flow velocity to the driving total energy gradient. The flow velocity for Newtonian fluids in laminar flow through cylindrical tubes is proportional to the square of the tube diameter (Hagen–Poiseuille equation). The Kozeny–Carman model considers the porous medium as a set of parallel cylindrical tubes and uses the Hagen–Poiseuille equation to compute the effective flow velocity (Kozeny, 1927; Carman, 1997). Then, the resulting permeability k (m^2) is proportional to the

square of the pore diameter D (m) and the porosity of the porous medium ϕ (m^3/m^3):

$$k = \frac{\phi}{32\tau^2} D^2 \quad (1)$$

where τ (m/m) is the tortuosity. However, pore size is not constant, and the largest interconnected pores are responsible for most of the flow. This is confirmed by network model studies of flow behavior at the pore scale, which show the coupling between pore size, spatial variability, and connectivity on flow patterns (Jang et al., 2011). Semiempirical factors added to the Kozeny–Carman equation attempt to take these processes into consideration, often through a generic tortuosity factor (equation 1).

Carbonate rocks store half of the world's proven oil reserves (US Energy Information Administration, 2015). Genesis and postdepositional diagenetic processes define the pore structure in carbonate rocks (Moore and Wade, 2013). The intraparticle porosity, high friability, and chemical reactivity of carbonate sediments affect their evolution during burial (Croizé et al., 2013; Moore and Wade, 2013) and leads to features such as dual and occluded porosity (Figure 1; see also Saner and Sahin, 1999; Poursoltani and Gibling, 2011). Experimental data show that the pore size in carbonates varies by more than 6 orders of magnitude (Nelson, 2009), whereas the permeability varies by approximately 10 orders

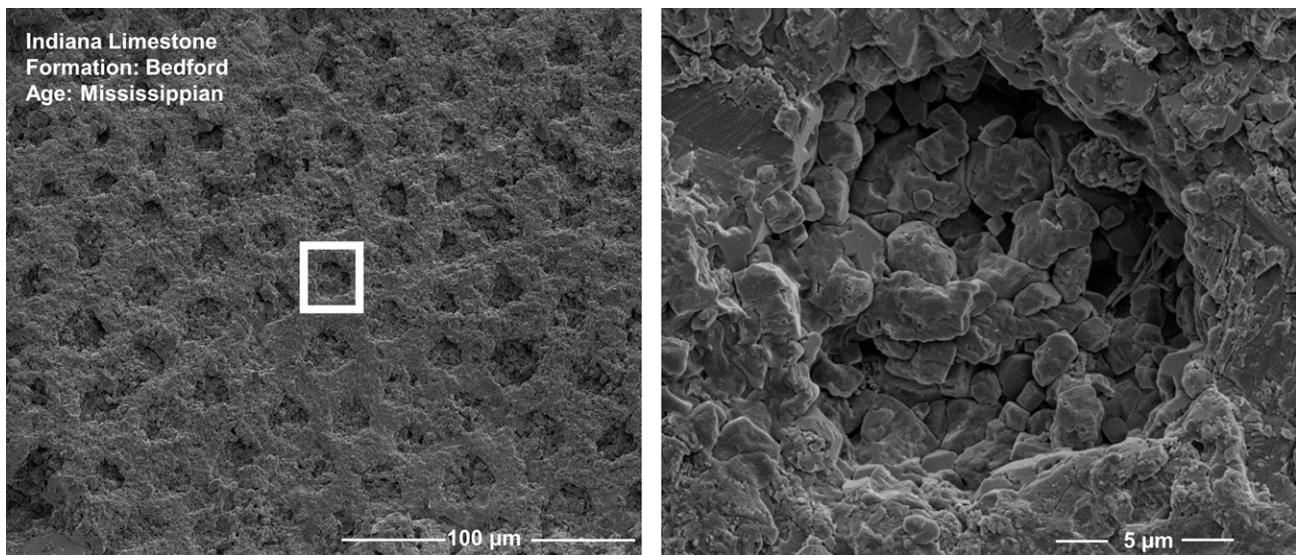


Figure 1. Scanning electron microscope image of an Indiana carbonate sample. The image confirms the presence of approximately 15 μm pores in agreement with mercury intrusion data. The zoomed-in picture on the right (corresponding to the white square on the left image) illustrates the submicron pore topology.

of magnitude (Nelson, 1994), which is in overall agreement with the power-2 dependency anticipated by equation 1.

The purpose of this study is to enhance the understanding of carbonate permeability using a physics-inspired yet data-driven approach. The following section describes the database compiled for this study.

DATABASE: CHARACTERIZATION AND POTENTIAL PITFALLS

This study compiles a database of permeability values extracted from published sources for carbonate rocks in the United States, Russia, the Middle East, and Europe (data sources are Brooks and Purcell, 1952; Chilingarian et al., 1990; Lucia, 1995; Mortensen et al., 1998; Lindsay et al., 2006; Fabricius et al., 2007; Clerke, 2009; Alam et al., 2011; Vincent et al., 2011). The 286 entries include mostly binary data in terms of permeability, rock formation, porosity, specific surface, and/or pore-size distribution (see Table S1, supplementary material available as AAPG Datashare 115 at www.aapg.org/datashare). Permeability and specific surface data span several orders of magnitude. Although data sources use similar measurement methods (gas adsorption for specific surface and helium expansion for porosity), differences in test protocols, devices, and data analyses add variability to the data set.

Only 13 entries have all 3, that of porosity, pore-size distribution, and specific surface (Paris Basin in Vincent et al., 2011). This research conducts a focused experimental study designed to extend this data set using 11 commercially available carbonates cores (Kocurek Industries), some with multimodal pore-size distributions (refer to Table 1). Test details and potential pitfalls follow.

Porosity

Weight change upon liquid saturation provides the accessible porosity (American Petroleum Institute, 1998). The saturation procedure involved five steps: (1) vacuum, (2) CO₂ injection cycles used to replace the residual air inside the specimen, (3) vacuum, (4) injection of deaired-deionized water into the vessel,

and (5) several vacuum–pressure cycles. The specimen dry weight W_{dry} (g) and saturated weight W_{sat} (g) combine to determine the porosity ϕ using the mineral specific gravity G_s :

$$\phi = \frac{(W_{sat} - W_{dry})G_s}{W_{dry} + (W_{sat} - W_{dry})G_s} \quad (2)$$

Measured porosities range between $\phi = 0.11$ and $\phi = 0.53$ (Table 1).

Specific Surface

Several liquid- and gas-based methods were tested to determine specific surface. Whereas liquid adsorption measurements rely on gravimetric changes after lengthy equilibration times (Cerato and Lutenegger, 2002), gas adsorption with krypton emerged as the most adequate characterization procedure given the relatively low specific surface area of carbonates (Micromeritics accelerated surface area and porosimetry system 2420 in Beebe et al., 1945). The measured specific surface areas S_s range from 0.5 to 1.3 m²/g (2441–6347 ft²/lb). This coincides with reported values for carbonate rocks (Chilingarian et al., 1990; Vincent et al., 2011).

Tests were conducted with carbonates crushed to two different sizes. Results summarized in Table 1 show that the measured specific surface depends on crushed particle size although the external surface area is negligible in all cases (e.g., the external surface is 0.03 m²/g [146 ft²/lb] for 70- μ m grains). This suggests that sample crushing gives access to occluded porosity and creates new gas pathways (calibration tests showed equipment variability of <4%).

Pore-Size Distribution

Mercury intrusion porosimetry (MIP) measures the volume of mercury that invades the specimen as a function of pressure (Giesche, 2006). Mercury invades along percolating paths, and occluded porosity remains untested. The Young–Laplace equation relates the measured pressure to pore-throat size (León y León, 1998), whereas injected volumes correspond to pore bodies. Consequently, large pores may be

Table 1. Carbonate Formations Tested in This Study

Sample	Location	Formation	Age	Porosity	Specific Surface, m ² /g (ft ² /lb)		Permeability, md
					D < 74 μm	150 μm > D > 74 μm	
Austin Chalk	Central-southcentral Texas*	Austin Chalk*	Late Cretaceous*	0.28	0.93 (4541)	0.60 (2929)	2.1
Desert Pink	Garden City, Texas	—	Early Cretaceous	0.30	0.49 (2392)	0.61 (2978)	9.6
Edwards White	Edwards Plateau, Texas	Edwards [†]	Early Cretaceous	0.13	0.85 (4150)	0.66 (3222)	0.1
Edwards Yellow	Garden City, Texas	Edwards [†]	Early Cretaceous	0.29	0.57 (2783)	0.59 (2881)	27
Indiana 2–4	Oolitic, Indiana	Bedford [‡]	Mississippian	0.15	0.83 (4052)	—	0.9
Indiana 60	Oolitic, Indiana	Bedford [‡]	Mississippian	0.17	1.09 (5322)	0.84 (4101)	21
Indiana 70	Oolitic, Indiana	Bedford [‡]	Mississippian	0.16	1.24 (6054)	0.91 (4443)	220
Indiana 200	Oolitic, Indiana	Bedford [‡]	Mississippian	0.13	0.72 (3515)	1.13 (5517)	73
Mount Gambier	Southeast, Australia [§]	Whalers Bluff [§]	Pliocene [§]	0.53	1.17 (5712)	0.51 (2490)	4636
Silurian Dolomite	Thornton, Illinois	Racine	Silurian	0.11	0.84 (4101)	0.39 (1904)	1.9
Winterset	Redfield, Kansas	Dennis [#]	Missourian [#]	0.27	0.54 (2636)	0.80 (3906)	35

Abbreviations: — = no data; D = pore diameter.

*Corbett et al. (1987).

[†]Fisher and Rodda (1969).

[‡]Churcher et al. (1991).

[§]Kyser et al. (1998).

^{||}Weiner and Koster Van Groos (1976).

[#]Rallsback (1993).

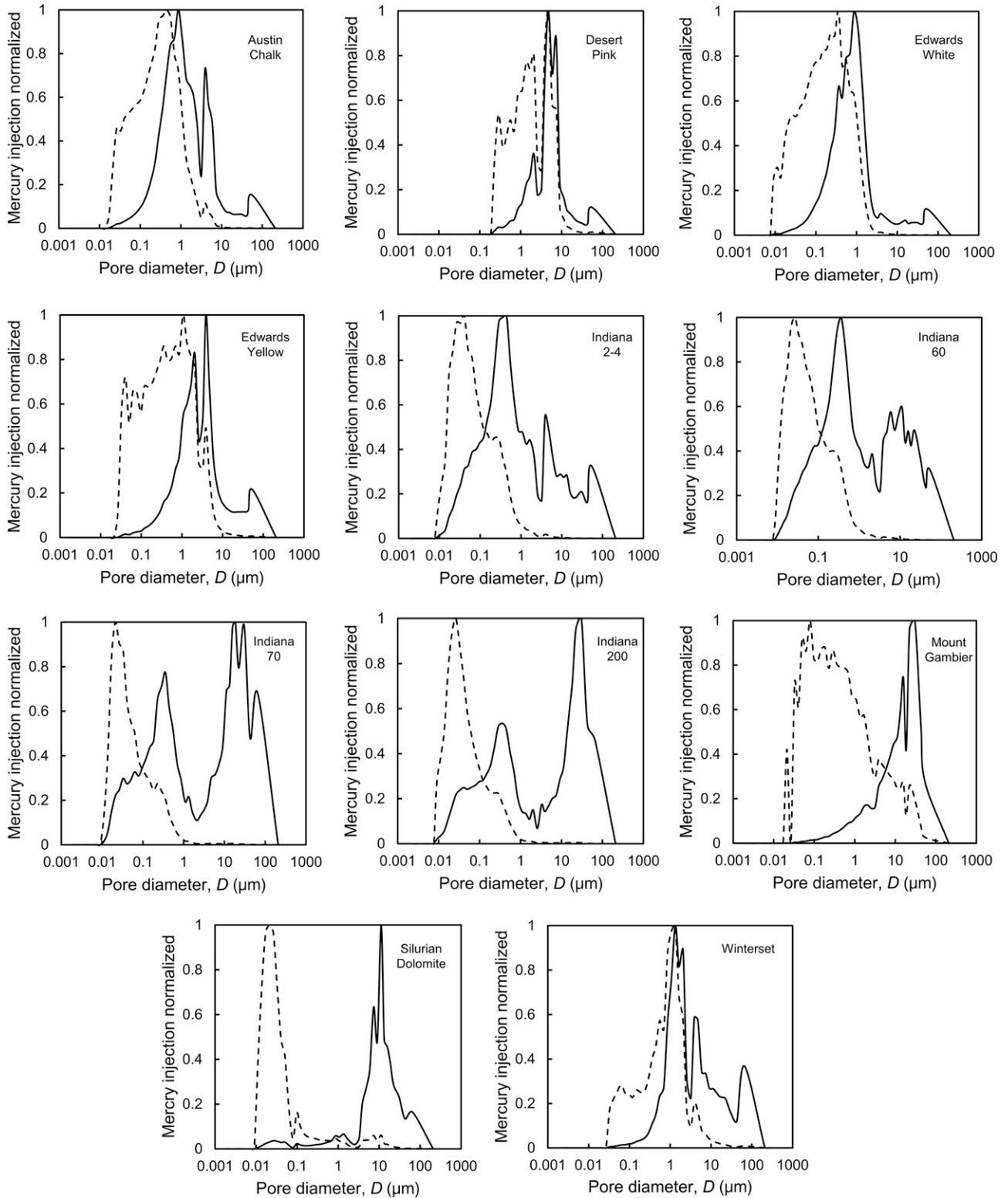


Figure 2. Normalized pore-size distributions obtained from mercury porosimetry. The black solid lines show the logarithmic differential intrusion, and the black dashed lines correspond to the probability density function.

assigned to small pore throats (i.e., the ink-bottle effect) (Diamond, 2000; Moro and Böhni, 2002).

Pore-size distributions obtained from mercury injection porosimetry tests are commonly presented in terms of pressure P (Pa) and the logarithm of the differential intrusion $g(D)$ for a given saturation S (m^3/m^3):

$$g(D) = \frac{dS}{d(\ln P)} = P \frac{dS}{dP} \quad (3)$$

This definition emphasizes dual porosity systems and amplifies the contribution of large pores. However, the physical pore-size density function $f(D)$ relates pressure to capillarity in terms of the surface tension γ (N/m [lbf/ft]) and the contact angle θ (rad) (Lenormand, 2003):

$$f(D) = \frac{P^2}{2\gamma \cos\theta} \frac{dS}{dP} = \frac{P}{2\gamma \cos\theta} g(D) = \frac{2}{D} g(D) \quad (4)$$

Therefore, the commonly used distribution $g(D)$ has a pore-size-dependent amplification of the true pore-size distribution $g(D) = D \times f(D)/2$. Figure 2 shows the pore-size distributions $g(D)$ and $f(D)$ obtained for the 11 specimens tested in this study. The estimated mean pore sizes computed from $g(D)$ are significantly smaller than the mean pore sizes obtained from $f(D)$. These results highlight profound differences in the potential interpretation of these data.

Permeability

The permeability of all 11 specimens was measured using a gas permeameter (MetaRock Laboratories SSK-300). The ends remained unpolished to avoid fines clogging near the inlet face of the cylindrical specimens (diameter was 25 mm [1 in.] and length was 50 mm [2 in.]), and limited pressure gradients prevented nonlinear effects. Values of N_2 permeability measured at different mean pressures were used to correct for Klinkenberg's effect. Table 1 includes the measured permeability values.

DATA ANALYSES

Porosity and Carbonate Classification

Empirical models for carbonate permeability focus on porosity as a predictive parameter (Jennings and Lucia, 2003; Babadagli and Al-Salmi, 2004; Lucia, 2007). The inherent limitation in empirical models that are based exclusively on porosity is highlighted by the contrast between the very narrow range in porosity (e.g., $0.1 < \phi < 0.6$) versus the 10 orders of magnitude in the permeability range (Nelson, 1994).

Additional information can be included, such as carbonate classification in terms of textural features and particle size, because these features provide

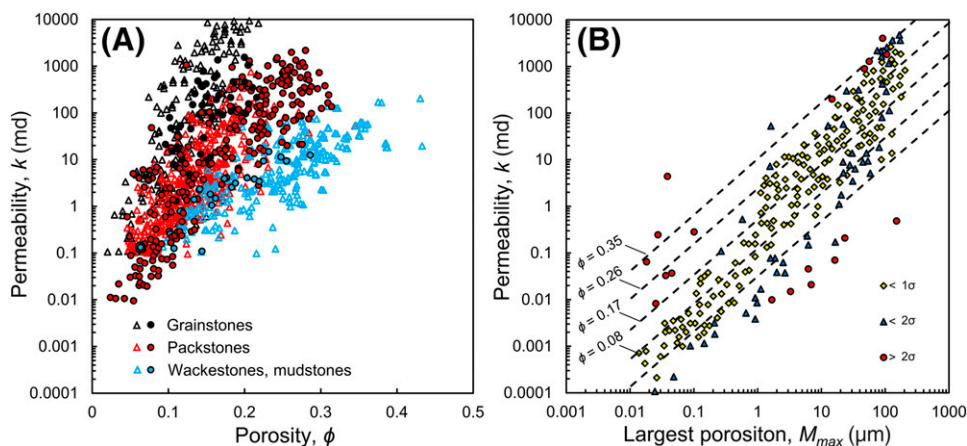


Figure 3. Empirical models for carbonate permeability. (A) Permeability as a function of porosity ϕ and carbonate type (data from Lucia, 1995 and Lindsay et al., 2006; for comparison, the original classification used by Lindsay et al., 2006 is mapped onto the classification from Lucia, 1995). Color coding identifies rock type; triangles correspond to data from Lucia, 1995 and filled circles are data from Lindsay et al., 2006. (B) Permeability as a function of the largest porosity size M_{max} measured using mercury porosimetry (after Clerke, 2009); dashed lines correspond to isoporosity values in the model (refer to equation 6). Data points are colored to reflect the distance between the model predictions and measured values in terms of standard deviation σ .

information about genesis and ensuing pore topology (Pemberton and Gingras, 2005; Boggs, 2009; Uddin et al., 2017).

The classification in Dunham (1962) distinguishes (1) coarse-grained dominant carbonates (grainstones being dolograins and large crystalline grainstones), (2) carbonates with a coarse-grained structure but with fines in pores (packstones), and (3) fines-dominant carbonates (wackestone, mudstone, and fine crystalline limestones and dolostones). Then, the empirical permeability–porosity power model (Lucia, 1995)

$$k = a \phi^b \quad (5)$$

relates the a factor and b exponent to carbonate rock type. Figure 3A superimposes two data sets for nonvuggy carbonate reservoirs in the United States and in the Middle East (Lucia, 1995; Lindsay et al., 2006). The model in Lucia (1995) highlights the importance of rock type and the impact of fines or “mud” on pore networks and permeability, yet predictions have more than one order of magnitude in uncertainty, which is in part because of potential differences in pore structure (see thin-section–based analyses in Weger et al., 2009).

Porosity, Pore-Size Distribution, and Pore Structure

Other models relate permeability to pore-size distributions inferred from mercury porosimetry (Swanson, 1981; Katz and Thompson, 1986; Glover et al., 2006; Rezaee et al., 2006; Gao and Hu, 2013). Data analyses reveal that the largest modal element or “porositon” M_{max} (μm) determines the matrix permeability (md) in carbonates with multimodal pore-size distributions (Figure 3B; Clerke et al., 2008; Clerke, 2009):

$$\log(k) = -1.54 + 1.2 \log(M_{max}) + 7.3\phi \quad (6)$$

More detailed analyses assume an internal pore structure such as fractal, consider critical path analysis, and/or apply percolation theory (Charlaix et al., 1987; Friedman and Seaton, 1998; Hunt and Gee, 2002; Buiting and Clerke, 2013; Daigle, 2016). For example, Buiting and Clerke (2013) match mercury porosimetry data with one or more Thomeer hyperbolas and extract three parameters: the maximum invaded volume ϕ^* , pressure at first invasion P_d (kPa), and

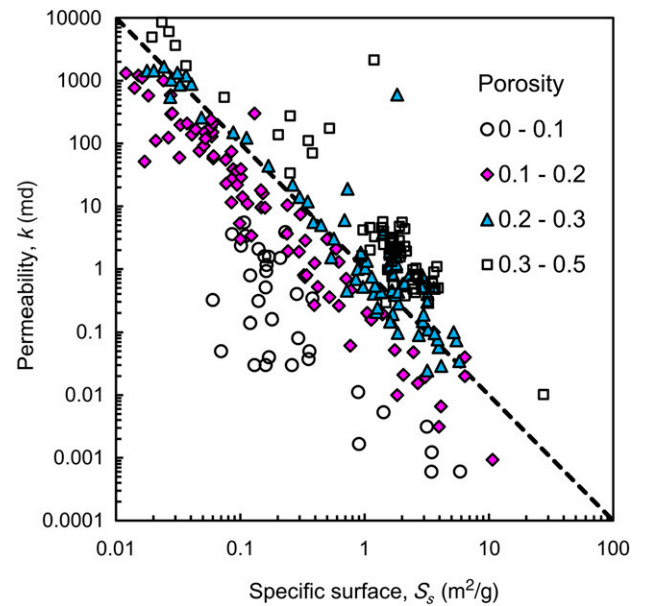


Figure 4. The permeability k versus specific surface S_s for different porosity ranges. The dashed line has a -2 slope in agreement with the Kozeny–Carman equation. The color coding distinguishes data points according to porosity. The data set includes 286 data points. The data sources are Brooks and Purcell (1952), Chilingarian et al. (1990), Mortensen et al. (1998), Fabricius et al. (2007), Alam et al. (2011), and Vincent et al. (2011).

pore geometry factor G . Through mathematical analysis, these three parameters combine to predict the rock permeability (assumes tortuosity is at ~ 2 and fractal dimension is at ~ 1.56 ; see resemblance with the earlier empirical models by Swanson, 1981 and Thomeer, 1983):

$$k = 24,050 \frac{\phi^*}{(P_d)^2} e^{-4.43\sqrt{G}} \quad (7)$$

where permeability is in darcys. The application of models based on pore-size distribution derived from MIP is not straightforward (starting from the interpretation of pore-size distribution data discussed above; equation 4). Although authors tend to highlight model predictability, results obtained as part of this study using these models against the data set show at least one order of magnitude in uncertainty.

Porosity and Specific Surface

Permeability is a measure of the drag that a viscous fluid experiences as it traverses a porous medium. Therefore, the data compilation and the experimental data set include specific surface and porosity. Data

Surface-related pore size D_{sur}

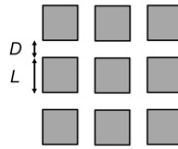
Assumptions/Comments

$$D_{sur} = \alpha \left[\frac{\phi}{(1-\phi) S_s \rho} \right]$$

General form

α is the structure factor

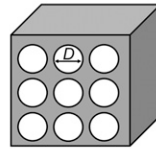
$$D_{sur} = 2 \left[\frac{\phi}{(1-\phi) S_s \rho} \right]$$



Simple cubic packing of cubical particles

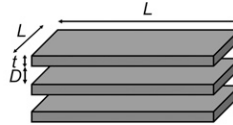
$D \ll L$

$$D_{sur} = 4 \left[\frac{\phi}{(1-\phi) S_s \rho} \right]$$



Pores are parallel cylindrical tubes

$$D_{sur} = 2 \left[\frac{\phi}{(1-\phi) S_s \rho} \right]$$



Parallel sheets

Figure 5. Models to estimate the surface-related pore size D_{sur} for different pore geometries where S_s (m^2/g) is specific surface and ϕ is porosity. ρ = mass density; D = pore diameter; L = largest grain size; t = grain thickness.

reported in terms of the volumetric specific surface S_{vol} (m^2/cm^3) are converted to the gravimetric specific surface S_s (m^2/g) as

$$S_s = \frac{1}{(1-\phi)\rho} S_{vol} \quad (8)$$

where ρ (g/cm^3) is the mass density of solids. Figure 4 illustrates permeability versus specific surface on a log-log scale. Data subsets of equal porosity cluster along lines with a slope of -2 in the log-log plot.

The Kozeny–Carman equation highlights the importance of pore size on permeability (equation 1). The specific surface S_s , porosity ϕ , and mineral mass density ρ combine to estimate the pore size D_{sur} (m) that corresponds to the measured surface area:

$$D_{sur} = \alpha \left[\frac{\phi}{(1-\phi) S_s \rho} \right] \quad (9)$$

where the α factor is a function of the fabric and pore topology, as shown in Figure 5. Figure 6 plots permeability values in the database as a function of the pore size estimated with equation 9 for $\alpha = 4$ (i.e., parallel cylindrical tubes; Figure 5). All data points cluster along a single trend with a slope of 2 in a log-log scale in agreement with the Kozeny–Carman model in equation 1 (see analogous conclusions for a wide range of sediments in Ren and

Santamarina, 2018). Most values fall within one order of magnitude of the main trend. The best fit line is

$$k = 5(D_{sur})^2 \quad (10)$$

where D_{sur} is in micrometers and permeability is in millidarcy. This equation allows us to predict permeability from S_s and ϕ values determined from small samples such as cuttings when pores are significantly smaller than the cutting size. In carbonates, the size of cuttings ranges from 1 to 10 mm (0.04–0.4 in.) long depending on drilling conditions (Archie, 1952; Dogruoz et al., 2016); therefore, cuttings are approximately three orders of magnitude larger than pores. However, cuttings impose an inherent bias because they break preferentially along more porous and weaker planes; therefore, predicted permeabilities are lower-bound estimates of the formation permeability.

DISCUSSION

Representative Pore Size

Out-of-trend data points in Figure 6 suggest that the pore size D_{sur} estimated from porosity and specific surface may not be an accurate predictor of the pore size that controls permeability in all cases.

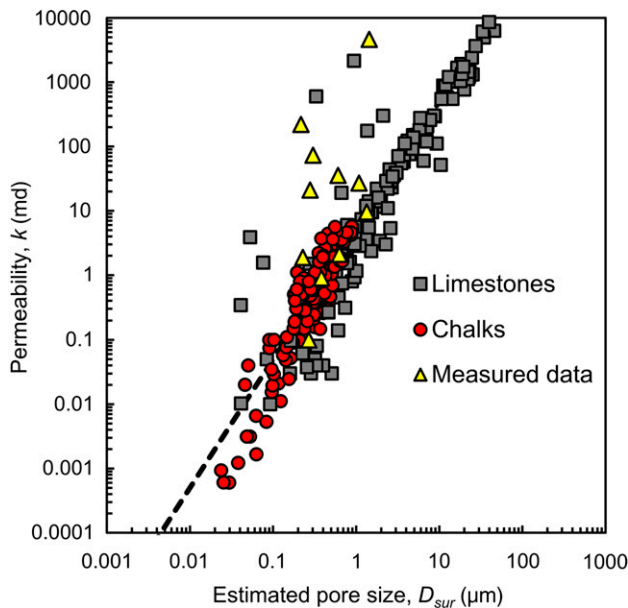


Figure 6. Measured permeability k versus estimated pore size D_{sur} using a model of parallel cylindrical tubes (equation 9). Most of the data collapse onto a narrow trend. The dashed line has a slope value of 2 in agreement with the Kozeny–Carman equation. The data sources are Brooks and Purcell (1952), Chilingarian et al. (1990), Mortensen et al. (1998), Fabricius et al. (2007), Alam et al. (2011), and Vincent et al. (2011). New experimental data gathered in this study are shown as yellow points.

Discordant data points either have clear dual porosity (see the $g(D)$ representation for Indiana 60, Indiana 70, and Indiana 200 in Figure 2) or they exhibit very broad pore-size distributions with long tails (Mount Gambier, Silurian Dolomite, and Winterset specimens in Figure 2).

The representative pore size that is most predictive of permeability is explored in Figure 7 in which the measured permeability values are plotted against selected pore diameter percentiles from $f(D)$ signatures (equation 4) (note that the representative pore size for permeability is equivalent to the concept of critical pore size in other studies; Arns et al., 2005; Nishiyama and Yokoyama, 2017). The data set used for this analysis includes the 11 samples tested in this study plus 13 carbonate samples from the literature (Vincent et al., 2011). The computed square error and visual inspection confirm that the pore size between the 70th and 85th percentiles in porosimetry data provides the most predictive permeability versus pore-size regression (micrometers) for all specimens (data range: $0.1 \text{ md} < k < 10,000 \text{ md}$):

$$k = 0.2(D80)^{1.75} \approx 0.1(D80)^2 \quad (11)$$

Although the first equation is the best fit, the second expression has a very similar residual error, and it is quadratic on the particle diameter in agreement with the Kozeny–Carman equation 1. The pore size estimate D_{sur} is less relevant to permeability in the discordant data points because flow channels along the larger interconnected pores (i.e., D80 percentile). Further analyses show that permeability estimates using the D80 pore size have the same degree of uncertainty (i.e., one order of magnitude) as more complex models that assume fractal pore structures, critical path analysis, and percolation theory (methods by Charlaix et al., 1987; Buiting and Clerke, 2013; Daigle, 2016).

Equations 10 and 11 indicate that the representative pore size D80 along the most conductive percolating paths is $D80/D_{sur} \approx 50$ larger than the pore size inferred from specific surface D_{sur} . The data set confirms the inverse relationship between specific surface and pore size; however, the pore size D_{sur} computed from the specific surface correlates best with the 20th percentile of the pore-size distribution $f(D)$ measured with mercury intrusion.

Anisotropy

Porosity, pore-size distribution, and specific surface do not provide information about anisotropy. Therefore, all models based on these parameters considered permeability to be isotropic (i.e., a scalar). However, permeability is direction dependent (i.e., a tensor). Permeability anisotropy in carbonates originates from inherent sedimentation layering and preferentially aligned features (Dürrast and Siegesmund, 1999; Tipping et al., 2006), biogenic burrows (Pemberton and Gingras, 2005), stress anisotropy (Barton and Quadros, 2014), and ensuing stress-dependent diagenetic processes (Sibson, 1994; Rashid et al., 2015; Toussaint et al., 2018).

Upscaling

Predictions based on MIP depend on the measurement and interpretation of pressure–volume data obtained on small specimens. The assumption of a fractal pore structure provides a convenient framework for upscaling laboratory measurements but only within the validity of the fractal system in the

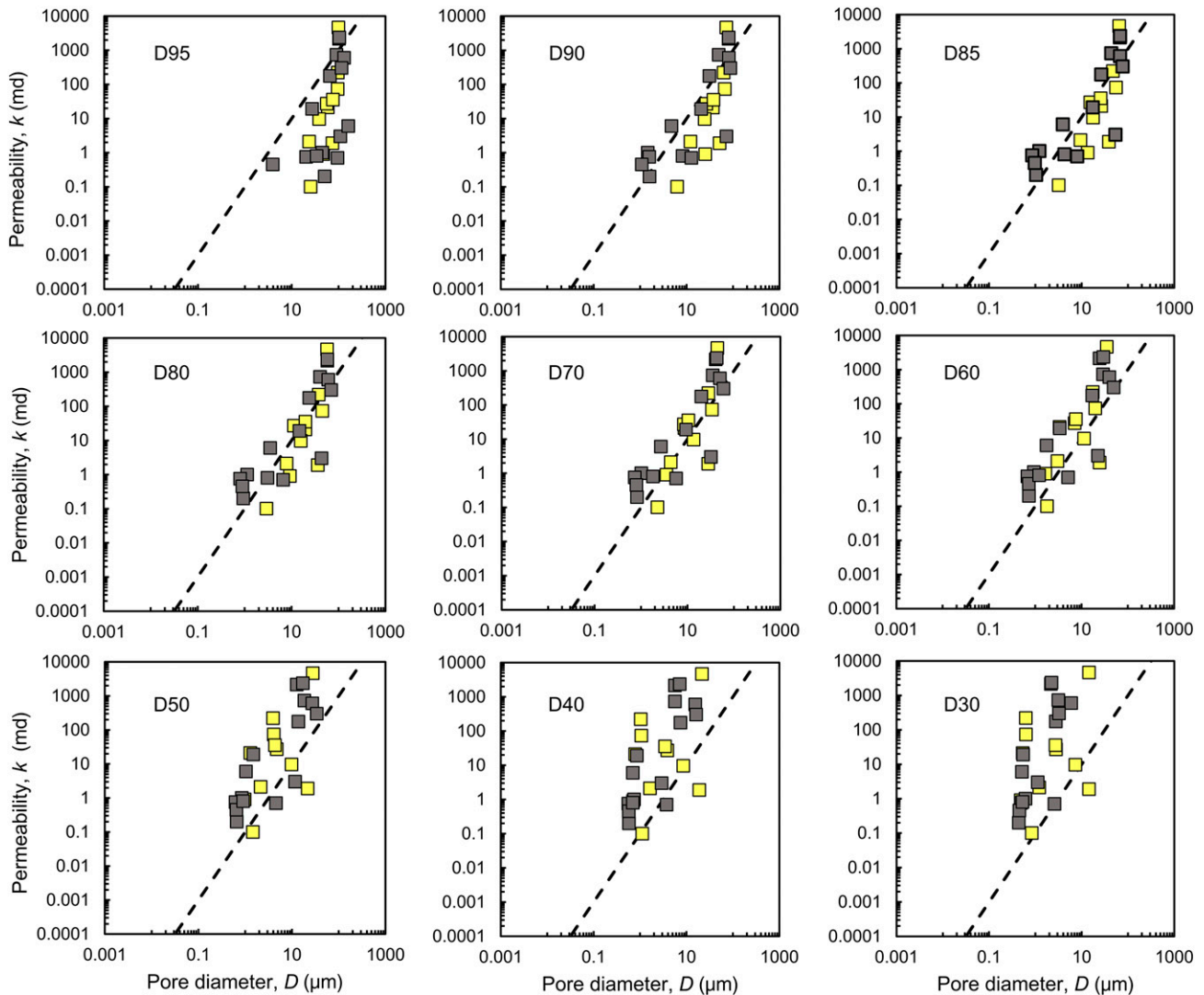


Figure 7. Permeability k versus different pore diameter D percentiles. The dashed line has a slope value of 2. The 70th to 85th percentiles in pore-size distributions (D70 to D85) provide the best regression with lowest square error with respect to the dashed line. New experimental data gathered in this study are shown as yellow points. Gray points indicate published data (Vincent et al., 2011).

rock matrix (Katz and Thompson, 1985; Pape et al., 1999; Costa, 2006). Stratigraphic features and fractures limit the upscaling size.

Alternatives

Analyses suggest that inherent limitations in the prediction of carbonate permeability from index properties lead to an uncertainty of at least one order of magnitude. Furthermore, porosity, specific surface, and porosimetry are costly measurements. They are most valuable when specimens are limited to small sizes, such as cuttings (Swanson, 1981; Santarelli

et al., 1998). However, when cores are available, quick liquid-based measurements of permeability can be less costly. These measurements avoid complex data analysis (as in gas-based measurements) (Wu et al., 1998; Tanikawa and Shimamoto, 2009; Sander et al., 2017) and provide the true value of permeability rather than a correlated estimate; additionally, the test series can readily assess anisotropy and heterogeneity.

CONCLUSIONS

Matrix flow is important even in fractured systems because hydrocarbons stored in the matrix need to

migrate to fractures. Carbonate type and formation history define the matrix permeability.

Permeability data plotted against the pore size estimated using porosity and specific surface cluster along a single trend with a slope of 2 (in log–log scale). This result highlights the underlying physics of permeability as captured in the Kozeny–Carman model.

Out-of-trend data points correspond to carbonates with either multimodal or broad pore-size distributions with long tails. In both cases, flow channels along the larger interconnected pores. Permeability correlates best with the pore size D80. This conclusion applies to all carbonates in the database, and it leads to a simple and robust permeability estimator.

More detailed analyses assume an internal pore structure and concepts such as critical path analysis. Their implementation is not straightforward; estimates of permeability using these models result in permeability values with a typical one order of magnitude in uncertainty. This variability is similar to that obtained with other simpler estimators.

All analyses suggest an irreducible uncertainty of one order of magnitude in permeability estimation from index properties such as porosity, porosimetry, and specific surface. This may reflect specimen preparation effects (e.g., crushing size for specific surface measurements or inadequate saturation in porosity determinations), inherent physical differences (permeation of single-phase fluid vs. invasion of an immiscible fluid in MIP), and difficulties in data interpretation (e.g., porosimetry, gas-related corrections in k measurements).

The estimation of permeability based on specific surface and porosity is most valuable when only cuttings are available. When cores are available, simple and quick liquid-based permeability measurements should be sought; they can be less costly than specific surface, porosity, and mercury porosimetry measurements, avoid the inherent uncertainty in correlation-based estimates, and allow the assessment of anisotropy.

REFERENCES CITED

- Alam, M. M., I. L. Fabricius, and M. Prasad, 2011, Permeability prediction in chalks: AAPG Bulletin, v. 95, no. 11, p. 1991–2014, doi:10.1306/03011110172.
- American Petroleum Institute, 1998, Recommended practices for core analysis, 2nd ed.: Washington, DC, API Publishing Services, 233 p.
- Archie, G. E., 1952, Classification of carbonate reservoir rocks and petrophysical considerations: AAPG Bulletin, v. 36, no. 2, p. 278–298.
- Arns, C. H., M. A. Knackstedt, and N. S. Martys, 2005, Cross-property correlations and permeability estimation in sandstone: Physical Review E, v. 72, no. 4, p. 046304, doi:10.1103/PhysRevE.72.046304.
- Babadagli, T., and S. Al-Salmi, 2004, A review of permeability-prediction methods for carbonate reservoirs using well-log data: SPE Reservoir Evaluation & Engineering, v. 7, no. 2, p. 75–88, doi:10.2118/87824-PA.
- Barton, N., and E. Quadros, 2014, Anisotropy is everywhere, to see, to measure, and to model: Rock Mechanics and Rock Engineering, v. 48, no. 4, p. 1323–1339, doi:10.1007/s00603-014-0632-7.
- Beebe, R. A., J. B. Beckwith, and J. M. Honig, 1945, The determination of small surface areas by krypton adsorption at low temperatures: Journal of the American Chemical Society, v. 67, no. 9, p. 1554–1558, doi:10.1021/ja01225a048.
- Boggs, S. Jr., 2009, Petrology of sedimentary rocks, 2nd ed.: Cambridge, United Kingdom, Cambridge University Press, 600 p., doi:10.1017/CBO9780511626487.
- BP, 2018, BP energy outlook, accessed February 10, 2019, <https://www.bp.com/content/dam/bp/business-sites/en/global/corporate/pdfs/energy-economics/energy-outlook/bp-energy-outlook-2018.pdf>.
- Brooks, C. S., and W. R. Purcell, 1952, Surface area measurements on sedimentary rocks: Fall Meeting of the Petroleum Branch of American Institute of Mining and Metallurgical Engineers, Houston, Texas, October 1–3, 1952, SPE-222-G, 12 p., doi:10.2118/222-G.
- Buiting, J. J. M., and E. A. Clerke, 2013, Permeability from porosimetry measurements: Derivation for a tortuous and fractal tubular bundle: Journal of Petroleum Science Engineering, v. 108, p. 267–278, doi:10.1016/j.petrol.2013.04.016.
- Carman, P. C., 1997, Fluid flow through granular beds: Chemical Engineering Research and Design, v. 75, p. S32–S48, doi:10.1016/S0263-8762(97)80003-2.
- Cerato, A. B., and A. J. Lutenegeger, 2002, Determination of surface area of fine-grained soils by the ethylene glycol monoethyl ether (EGME) method: Geotechnical Testing Journal, v. 25, no. 3, p. 315–321, doi:10.1520/GTJ11087J.
- Charlaix, E., E. Guyon, and S. Roux, 1987, Permeability of a random array of fractures of widely varying apertures: Transport in Porous Media, v. 2, no. 1, p. 31–43, doi:10.1007/BF00208535.
- Chilingarian, G. V., J. Chang, and K. I. Bagrintseva, 1990, Empirical expression of permeability in terms of porosity, specific surface area, and residual water saturation of carbonate rocks: Journal of Petroleum Science Engineering, v. 4, no. 4, p. 317–322, doi:10.1016/0920-4105(90)90029-3.
- Churcher, P. L., P. R. French, J. C. Shaw, and L. L. Schramm, 1991, Rock properties of Berea Sandstone, Baker Dolomite,

- and Indiana Limestone: SPE International Symposium on Oilfield Chemistry, Anaheim, California, February 20–22, 1991, SPE-21044-MS, 19 p., doi:[10.2118/21044-MS](https://doi.org/10.2118/21044-MS).
- Clerke, E. A., 2009, Permeability, relative permeability, microscopic displacement efficiency and pore geometry of M₁ bimodal pore systems in Arab-D limestone: SPE Journal, v. 14, p. 524–531, doi:[10.2118/105259-PA](https://doi.org/10.2118/105259-PA).
- Clerke, E. A., H. W. Mueller III, E. C. Phillips, R. Y. Eyvazzadeh, D. H. Jones, R. Ramamoorthy, and A. Srivastava, 2008, Application of Thomeer hyperbolas to decode the pore systems, facies and reservoir properties of the Upper Jurassic Arab D Limestone, Ghawar field, Saudi Arabia: A “Rosetta Stone” approach: GeoArabia, v. 13, no. 4, p. 113–160.
- Corbett, K., M. Friedman, and J. Spang, 1987, Fracture development and mechanical stratigraphy of Austin Chalk, Texas: AAPG Bulletin, v. 71, no. 1, p. 17–28.
- Costa, A., 2006, Permeability-porosity relationship: A re-examination of the Kozeny-Carman equation based on a fractal pore-space geometry assumption: Geophysical Research Letters, v. 33, no. 2, p. L02318, doi:[10.1029/2005GL025134](https://doi.org/10.1029/2005GL025134).
- Croizé, D., F. Renard, and J.-P. Gratier, 2013, Compaction and porosity reduction in carbonates: A review of observations, theory and experiments: Advances in Geophysics, v. 54, p. 181–238, doi:[10.1016/B978-0-12-380940-7.00003-2](https://doi.org/10.1016/B978-0-12-380940-7.00003-2).
- Daigle, H., 2016, Application of critical path analysis for permeability prediction in natural porous media: Advances in Water Resources, v. 96, p. 43–54, doi:[10.1016/j.advwatres.2016.06.016](https://doi.org/10.1016/j.advwatres.2016.06.016).
- Diamond, S., 2000, Mercury porosimetry: An inappropriate method for the measurement of pore size distributions in cement-based materials: Cement and Concrete Research, v. 30, no. 10, p. 1517–1525, doi:[10.1016/S0008-8846\(00\)00370-7](https://doi.org/10.1016/S0008-8846(00)00370-7).
- Dogruoz, C., N. Bolukbasi, J. Rostami, and C. Acar, 2016, An experimental study of cutting performances of worm picks: Rock Mechanics and Rock Engineering, v. 49, no. 1, p. 213–224, doi:[10.1007/s00603-015-0734-x](https://doi.org/10.1007/s00603-015-0734-x).
- Dullien, F. A. L., 1992, Porous media: Fluid transport and pore structure, 2nd ed.: San Diego, California, Academic Press, 574 p.
- Dunham, R. J., 1962, Classification of carbonate rocks according to depositional textures, in W. E. Ham, ed., Classification of carbonate rocks--A symposium: AAPG Memoir 1, p. 108–121.
- Dürrast, H., and S. Siegesmund, 1999, Correlation between rock fabrics and physical properties of carbonate reservoir rocks: International Journal of Earth Sciences, v. 88, no. 3, p. 392–408, doi:[10.1007/s005310050274](https://doi.org/10.1007/s005310050274).
- Fabricius, I. L., G. Baechle, G. P. Eberli, and R. Weger, 2007, Estimating permeability of carbonate rocks from porosity and vp/vs: Geophysics, v. 72, no. 5, p. E185–E191, doi:[10.1190/1.2756081](https://doi.org/10.1190/1.2756081).
- Fisher, W. L., and P. U. Rodda, 1969, Edwards Formation (Lower Cretaceous), Texas: Dolomitization in a carbonate platform system: AAPG Bulletin, v. 53, no. 1, p. 55–72.
- Friedman, S. P., and N. A. Seaton, 1998, Critical path analysis of the relationship between permeability and electrical conductivity of three-dimensional pore networks: Water Resources Research, v. 34, no. 7, p. 1703–1710, doi:[10.1029/98WR00939](https://doi.org/10.1029/98WR00939).
- Gale, J. F. W., S. E. Laubach, R. A. Marrett, J. E. Olson, J. Holder, and R. M. Reed, 2004, Predicting and characterizing fractures in dolostone reservoirs: Using the link between diagenesis and fracturing, in C. J. R. Braithwaite, G. Rizzi, and G. Darke, eds., The geometry and petrogenesis of dolomite hydrocarbon reservoirs: Geological Society, London, Special Publications 2004, v. 235, p. 177–192, doi:[10.1144/GSL.SP.2004.235.01.08](https://doi.org/10.1144/GSL.SP.2004.235.01.08).
- Gao, Z., and Q. Hu, 2013, Estimating permeability using median pore-throat radius obtained from mercury intrusion porosimetry: Journal of Geophysics and Engineering, v. 10, no. 2, p. 1–7, doi:[10.1088/1742-2132/10/2/025014](https://doi.org/10.1088/1742-2132/10/2/025014).
- Giesche, H., 2006, Mercury porosimetry: A general (practical) overview: Particle & Particle Systems Characterization, v. 23, no. 1, p. 9–19, doi:[10.1002/ppsc.200601009](https://doi.org/10.1002/ppsc.200601009).
- Glover, J. P. W., I. I. Zadjali, and K. A. Frew, 2006, Permeability prediction from MICP and NMR data using an electrokinetic approach: Geophysics, v. 71, no. 4, p. F49–F60, doi:[10.1190/1.2216930](https://doi.org/10.1190/1.2216930).
- Hunt, A. G., and G. W. Gee, 2002, Application of critical path analysis to fractal porous media: Comparison with examples from the Hanford site: Advances in Water Resources, v. 25, no. 2, p. 129–146, doi:[10.1016/S0309-1708\(01\)00057-4](https://doi.org/10.1016/S0309-1708(01)00057-4).
- International Energy Agency, 2015, World energy outlook 2015: Executive summary, accessed July 6, 2017, <https://webstore.iea.org/download/summary/224?fileName=English-WEO-2015-ES.pdf>.
- International Energy Agency, 2018, World energy outlook 2018: Executive summary, accessed February 10, 2019, <https://webstore.iea.org/download/summary/190?fileName=English-WEO-2018-ES.pdf>.
- Jang, J., G. A. Narsilio, and J. C. Santamarina, 2011, Hydraulic conductivity in spatially varying media—A pore-scale investigation: Geophysical Journal International, v. 184, no. 3, p. 1167–1179, doi:[10.1111/j.1365-246X.2010.04893.x](https://doi.org/10.1111/j.1365-246X.2010.04893.x).
- Jennings, J. W. Jr., and F. J. Lucia, 2003, Predicting permeability from well logs in carbonates with a link to geology for interwell permeability mapping: SPE Reservoir Evaluation & Engineering, v. 6, no. 4, p. 215–225, doi:[10.2118/84942-PA](https://doi.org/10.2118/84942-PA).
- Katz, A. J., and A. H. Thompson, 1985, Fractal sandstone pores: Implications for conductivity and pore formation: Physical Review Letters, v. 54, no. 12, p. 1325–1328, doi:[10.1103/PhysRevLett.54.1325](https://doi.org/10.1103/PhysRevLett.54.1325).
- Katz, A. J., and A. H. Thompson, 1986, Quantitative prediction of permeability in porous rock: Physical Review B, v. 34, no. 11, p. 8179–8181, doi:[10.1103/PhysRevB.34.8179](https://doi.org/10.1103/PhysRevB.34.8179).
- Kozeny, J., 1927, About capillary conduction of water in the soil (ascent, infiltration and application to irrigation) [in

- German]: Vienna, Austria, Academy of Sciences Meeting Report 136, p. 271–306.
- Kyser, T. K., N. P. James, and Y. Bone, 1998, Alteration of Cenozoic cool-water carbonates to low-Mg calcite in marine waters, Gambier Embayment, South Australia: *Journal of Sedimentary Research*, v. 68, no. 5, p. 947–955, doi:10.2110/jsr.68.947.
- Lenormand, R., 2003, Interpretation of mercury injection curves to derive pore size distribution: International Symposium of the Society of Core Analysts, Pau, France, September 21–24, 2003, 7 p.
- León y León, C. A., 1998, New perspectives in mercury porosimetry: *Advances in Colloid and Interface Science*, v. 76–77, p. 341–372, doi:10.1016/S0001-8686(98)00052-9.
- Lindsay, R. F., D. L. Cantrell, G. W. Hughes, T. H. Keith, H. W. Mueller III, and S. D. Russel, 2006, Ghawar Arab-D Reservoir: Widespread porosity in shoaling-upward carbonate cycles, Saudi Arabia, in P. M. Harris and L. J. Weber, eds., *Giant hydrocarbon reservoirs of the world: From rocks to reservoir characterization and modeling*: AAPG Memoir 88, p. 97–137.
- Lucia, F. J., 1995, Rock-fabric/petrophysical classification of carbonate pore space for reservoir characterization: *AAPG Bulletin*, v. 79, no. 9, p. 1275–1300, doi:10.1306/7834D4A4-1721-11D7-8645000102C1865D.
- Lucia, F. J., 2007, *Carbonate reservoir characterization: An integrated approach*, 2nd ed.: Berlin, Springer-Verlag, 336 p.
- Moore, C. H., and W. J. Wade, 2013, The nature and classification of carbonate porosity, in C. H. Moore and W. J. Wade, eds., *Carbonate reservoirs: Porosity and diagenesis in a sequence stratigraphic framework*, 2nd ed.: Amsterdam, Elsevier, *Developments in Sedimentology* 67, p. 51–65, doi:10.1016/B978-0-444-53831-4.00004-5.
- Moro, F., and H. Böhni, 2002, Ink-bottle effect in mercury intrusion porosimetry of cement-based materials: *Journal of Colloid and Interface Science*, v. 246, no. 1, p. 135–149, doi:10.1006/jcis.2001.7962.
- Mortensen, J., F. Engstrom, and I. Lind, 1998, The relation among porosity, permeability, and specific surface of chalk from the Gorm Field, Danish North Sea: *SPE Reservoir Evaluation & Engineering*, v. 1, p. 245–251, doi:10.2118/31062-PA.
- Nelson, P. H., 1994, Permeability-porosity relationships in sedimentary rocks: *The Log Analyst*, v. 35, no. 3, p. 38–62.
- Nelson, P. H., 2009, Pore-throat sizes in sandstones, tight sandstones, and shales: *AAPG Bulletin*, v. 93, no. 3, p. 329–340, doi:10.1306/10240808059.
- Nishiyama, N., and T. Yokoyama, 2017, Permeability of porous media: Role of the critical pore size: *Journal of Geophysical Research Solid Earth*, v. 122, no. 9, p. 6955–6971, doi:10.1002/2016JB013793.
- Ortega, O. J., J. F. W. Gale, and R. Marrett, 2010, Quantifying diagenetic and stratigraphic controls on fracture intensity in platform carbonates: An example from the Sierra Madre Oriental, northeast Mexico: *Journal of Structural Geology*, v. 32, no. 12, p. 1943–1959, doi:10.1016/j.jsg.2010.07.004.
- Pape, H., C. Clauser, and J. Iffland, 1999, Permeability prediction based on fractal pore-space geometry: *Geophysics*, v. 64, no. 5, p. 1447–1460, doi:10.1190/1.1444649.
- Pemberton, S. G., and M. K. Gingras, 2005, Classification and characterizations of biogenically enhanced permeability: *AAPG Bulletin*, v. 89, no. 11, p. 1493–1517, doi:10.1306/07050504121.
- Poursoltani, M. R., and M. R. Gibling, 2011, Composition, porosity, and reservoir potential of the Middle Jurassic Kashafrud Formation, northeast Iran: *Marine and Petroleum Geology*, v. 28, no. 5, p. 1094–1110, doi:10.1016/j.marpetgeo.2010.11.004.
- Railsback, L. B., 1993, Contrasting styles of chemical compaction in the Upper Pennsylvanian Dennis Limestone in the Midcontinent region, U.S.A.: *Journal of Sedimentary Petrology*, v. 63, no. 1, p. 61–72, doi:10.1306/D4267A8C-2B26-11D7-8648000102C1865D.
- Rashid, F., P. W. J. Glover, P. Lorinczi, R. Collier, and J. Lawrence, 2015, Porosity and permeability of tight carbonate reservoir rocks in the north of Iraq: *Journal of Petroleum Science Engineering*, v. 133, p. 147–161, doi:10.1016/j.petrol.2015.05.009.
- Ren, X. W., and J. C. Santamarina, 2018, The hydraulic conductivity of sediments: A pore size perspective: *Engineering Geology*, v. 233, p. 48–54, doi:10.1016/j.enggeo.2017.11.022.
- Rezaee, M. R., A. Jafari, and E. Kazemzadeh, 2006, Relationships between permeability, porosity and pore throat size in carbonate rocks using regression analysis and neural networks: *Journal of Geophysics and Engineering*, v. 3, no. 4, p. 370–376, doi:10.1088/1742-2132/3/4/008.
- Sander, R., Z. Pan, and L. D. Connell, 2017, Laboratory measurement of low permeability unconventional gas reservoir rocks: A review of experimental methods: *Journal of Natural Gas Science and Engineering*, v. 37, p. 248–279, doi:10.1016/j.jngse.2016.11.041.
- Saner, S., and A. Sahin, 1999, Lithological and zonal porosity-permeability distributions in the Arab-D Reservoir, Uthmaniyah Field, Saudi Arabia: *AAPG Bulletin*, v. 83, no. 2, p. 230–243.
- Santarelli, F. J., A. F. Marsala, M. Brignoli, E. Rossi, and N. Bona, 1998, Formation evaluation from logging on cuttings: *SPE Reservoir Evaluation & Engineering*, v. 1, p. 238–244.
- Sibson, R. H., 1994, *Crustal stress, faulting and fluid flow*: Geological Society, London, *Special Publications* 1994, v. 78, p. 69–84, doi:10.1144/GSL.SP.1994.078.01.07.
- Swanson, B. F., 1981, A simple correlation between permeabilities and mercury capillary pressures: *Journal of Petroleum Technology*, v. 33, p. 2498–2504, doi:10.2118/8234-PA.
- Tanikawa, W., and T. Shimamoto, 2009, Comparison of Klinkenberg-corrected gas permeability and water permeability in sedimentary rocks: *International Journal of Rock Mechanics and Mining Sciences*, v. 46, no. 2, p. 229–238, doi:10.1016/j.ijrmmms.2008.03.004.
- Thomeer, J. H., 1983, Air permeability as a function of three pore-network parameters: *Journal of Petroleum Technology*, v. 35, no. 4, p. 809–814, doi:10.2118/10922-PA.

- Tiab, D., and E. C. Donaldson, 2012, *Petrophysics: Theory and practice of measuring reservoir rock and fluid transport properties*, 3rd ed.: Boston, Gulf Professional Publishing, 976 p.
- Tipping, R. G., A. C. Runkel, E. C. Alexander Jr., S. C. Alexander, and J. A. Green, 2006, Evidence for hydraulic heterogeneity and anisotropy in the mostly carbonate Prairie du Chien Group, southeastern Minnesota, USA: *Sedimentary Geology*, v. 184, no. 3–4, p. 305–330, doi:10.1016/j.sedgeo.2005.11.007.
- Toussaint, R., E. Aharonov, D. Koehn, J.-P. Gratier, M. Ebner, P. Baud, A. Rolland, and F. Renard, 2018, Stylolites: A review: *Journal of Structural Geology*, v. 114, p. 163–195, doi:10.1016/j.jsg.2018.05.003.
- Uddin, Y. N., E. A. Clerke, B. Bammel, S. Koronfol, and A. Grader, 2017, Quantitative study of formation vertical permeability in Middle East Thalassinoides burrowed carbonate mudstone: SPE Reservoir Characterisation and Simulation Conference and Exhibition, Abu Dhabi, United Arab Emirates, May 8–10, 2017, SPE-186001-MS, 17 p.
- US Energy Information Administration, 2015, International energy statistics: Total primary energy production, accessed July 6, 2017, <https://www.eia.gov/beta/international/data/browser>.
- Van Golf-Racht, T. D., 1996, Naturally-fractured carbonate reservoirs, in G. V. Chilingarian, S. J. Mazzullo, and H. H. Rieke, eds., *Carbonate reservoir characterization: A geologic-engineering analysis*: Amsterdam, Elsevier, v. 44, pt. 2, p. 683–771, doi:10.1016/S0376-7361(96)80029-X.
- Vincent, B., M. Fleury, Y. Santerre, and B. Brigaud, 2011, NMR relaxation of neritic carbonates: An integrated petrophysical and petrographical approach: *Journal of Applied Geophysics*, v. 74, no. 1, p. 38–58, doi:10.1016/j.jappgeo.2011.03.002.
- Weger, R. J., G. P. Eberli, G. T. Baechle, J. L. Massafiero, and Y.-F. Sun, 2009, Quantification of pore structure and its effect on sonic velocity and permeability in carbonates: *AAPG Bulletin*, v. 93, no. 10, p. 1297–1317, doi:10.1306/05270909001.
- Weiner, W. F., and A. F. Koster Van Groos, 1976, Petrographic and geochemical study of the formation of chert around the Thornton reef complex, Illinois: *Geological Society of America Bulletin*, v. 87, no. 2, p. 310–318, doi:10.1130/0016-7606(1976)87<310:PAGSOT>2.0.CO;2.
- Wu, Y.-S., K. Pruess, and P. Persoff, 1998, Gas flow in porous media with Klinkenberg effects: *Transport in Porous Media*, v. 32, no. 1, p. 117–137, doi:10.1023/A:1006535211684.